

Electronic Supplementary Material (ESI) for Dalton Trans.

"Occurrence of slow relaxation of the magnetization in a family of copper(II)/manganese(II) quasi-isotropic complexes with different ground spin states."

Evangelos Pilichos,^a Mercè Font-Bardia,^b Albert Escuer,^{a,c*} Júlia Mayans,^{a,c*}

^a Departament de Química Inorgànica i Orgànica, Secció Inorgànica, Martí i Franquès 1-11, Barcelona-08028, Spain.

^b Departament de Mineralogia, Cristal·lografia i Dipòsits Minerals, Universitat de Barcelona, Martí Franqués s/n, 08028 Barcelona (Spain) and Unitat de Difracció de R-X. Centre Científic i Tecnològic de la Universitat de Barcelona (CCiTUB), Solé i Sabaris 1-3. 08028 Barcelona.

^c Institute of Nanoscience and Nanotechnology (IN²UB), Universitat de Barcelona.

1- IR spectra.

Fig. S1. IR spectra for **1-5**.

2- Structural aspects.

Table S1. Crystal data and structure refinement for complexes **1 - 5**.

Fig. S2. Coordination environment for the Mn^{II} cation in complexes **2-5**.

Table S2. Relevant donor-acceptor distances (Å) and donor-H···acceptor angles for the H-bonds present in complexes **1, 3, 4** and **5**.

3- Magnetic data.

Fig. S3. χ_M'' dependence of the transverse field for complexes **2** (top), **3** (middle) and **5** (bottom).

Fig. S4. Plot of $\ln(1/2\pi\nu)$ vs. T^1 from the $\chi_M''(T)$ data for complexes **2, 3** and **5**.

Fig. S5. $\chi_M''(T)$ for complexes **2, 3** and **5** showing the lower frequencies and high frequencies out-of-phase response.

Fig. S6. Cole-Cole plots for complexes **2, 3** and **5**.

1- IR spectra.

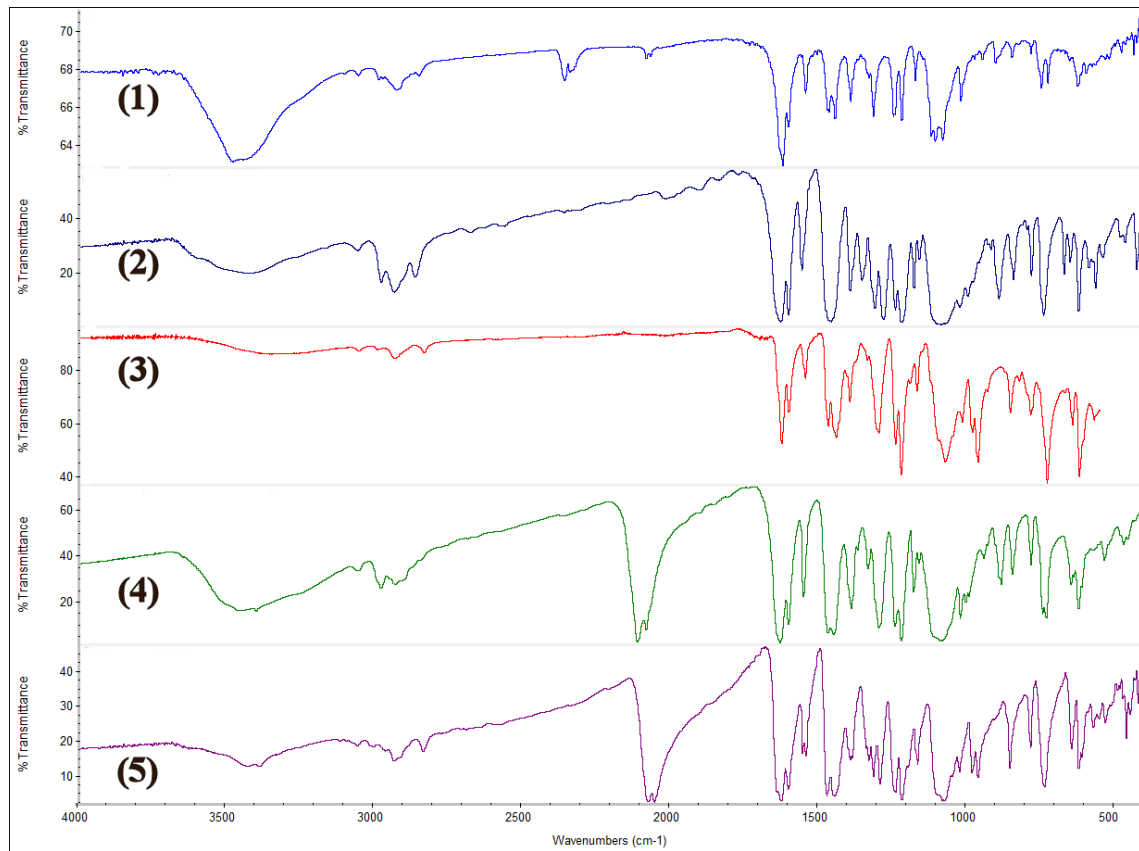


Fig. S1. IR spectra for complexes **1** - **5**. Characteristic bands: st. C-H 3000-2800 cm⁻¹; N=C iminic ~1600 cm⁻¹; C-O st. ClO₄⁻ 1075 cm⁻¹; δ ClO₄⁻ 620 cm⁻¹. Stretching for the azido ligands for **4** and **5** appears between 2050-2100 cm⁻¹. **2RR** and **2SS** exhibit superimposable spectra and only one spectrum is shown.

2-Structural aspects.

Table S1. Crystal data and structure refinement for complexes **1 - 5**.

	1	2SS 2CH ₂ Cl ₂ ·0.5MeOH	3 ·MeOH	4 ·2MeOH	5
Formula	C ₂₁ H ₂₆ ClCu N ₂ NaO ₉	C ₁₀₁ H ₁₂₈ Cl ₈ Cu ₄ Mn ₂ N ₈ O ₃₅	C ₅₆ H ₆₆ Cl ₂ Cu ₃ MnN ₆ O ₂₄	C ₈₂ H ₁₀₀ Cl ₂ Cu ₄ Mn ₂ N ₁₄ O ₂₈	C ₇₄ H ₈₀ Cl ₂ Cu ₄ Mn ₂ N ₂₀ Na ₂ O ₂₆
FW	572.42	2661.75	1523.60	2164.69	2146.5
System	Monoclinic	Triclinic	Monoclinic	Triclinic	Triclinic
Space group	P21/c	P 1	P21/c	P-1	P-1
<i>a</i> /Å	8.0671(4)	12.2722(6)	15.4787(6)	9.876(1)	12.3500(6)
<i>b</i> /Å	21.2492(9)	14.5327(7)	22.7556(9)	14.787(2)	13.0272(7)
<i>c</i> /Å	14.0782(7)	17.2926(8)	17.7148(7)	16.663(2)	13.9308(7)
α /deg.	90	101.148(2)	90	73.292(5)	107.897(2)
β /deg.	103.285(2)	100.531(2)	97.002(1)	83.822(5)	91.793(2)
γ /deg.	90	111.062(2)	90	70.888(5)	94.147(2)
<i>V</i> /Å ³	2348.7(2)	2714.5(2)	6193.1(4)	2201.8(5)	2123.9(2)
<i>Z</i>	4	1	4	1	1
<i>T</i> , K	100(2)	100(2)	100(2)	100(2)	100(2)
λ (MoK α), Å	0.71073	0.71073	0.71073	0.71073	0.71073
ρ_{calc} , g·cm ⁻³	1.619	1.628	1.634	1.633	1.678
μ (MoK α), mm ⁻¹	1.118	1.279	1.389	1.376	1.435
Flack param.	----	0.02(1)	----	----	----
<i>R</i>	0.0340	0.0481	0.0479	0.0490	0.0334
ωR^2	0.0718	0.1328	0.1094	0.1328	0.0889

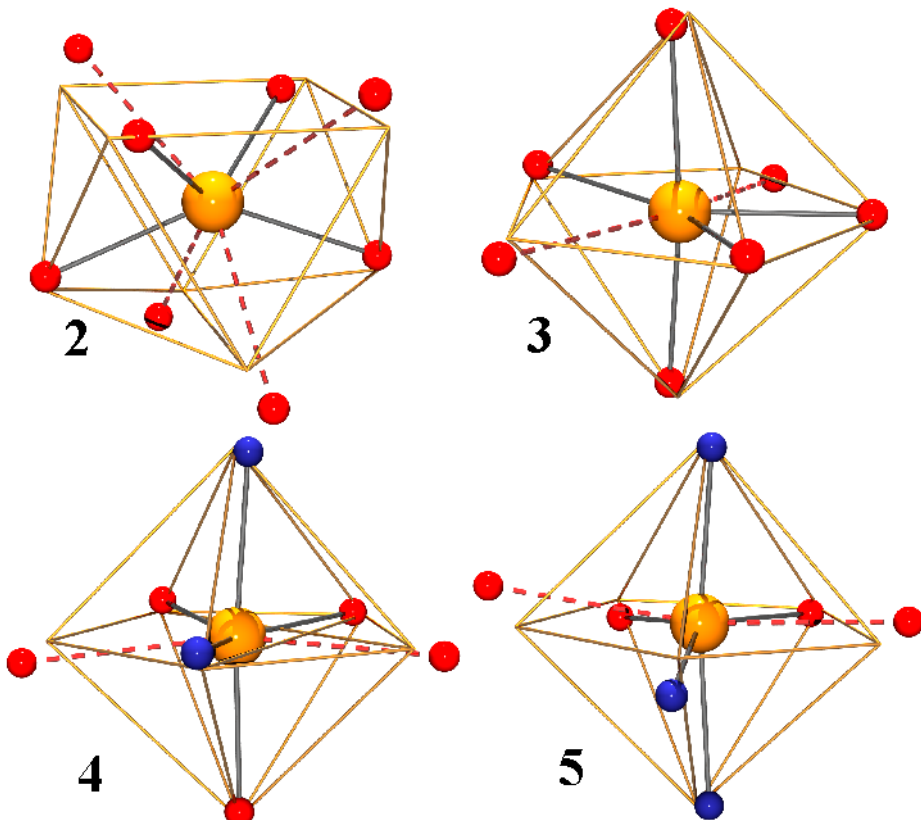


Fig. S2. Coordination environment for the Mn^{II} cation in complexes **2SS-5**. Dashed red bonds show the large contacts Mn-O_{alcoxo}. The ideal polyhedra (biapicated trigonal prism for **2SS** and pentagonal bipyramid for **3-5**) are shown in orange.

Table S2. Relevant donor-acceptor distances (\AA) and donor-H \cdots acceptor angles for the H-bonds present in complexes **1**, **3**, **4** and **5**. For **1** and **5** correspond to the intermolecular H-bonds that determines the 1D arrangement in the network whereas for **3** and **4** correspond to the intramolecular H-bonds between the central and the capping [CuL] fragments.

	D \cdots A (\AA)		D-H \cdots A (deg.)		
Complex 1	O9 \cdots O5'	2.831(2)	O9-H9O \cdots O5'	158.6(3)	Intermolecular
Complex 5	O8 \cdots N7'	2.843(2)	O8-H8O \cdots N7'	166(2)	
Complex 3	O13 \cdots O9	2.955(4)	O13-H13B \cdots O9	137(3)	Intramolecular
	O13 \cdots O10	2.806(3)	O13-H13B \cdots O10	148(3)	
	O13 \cdots O11	2.752(3)	O13-H13A \cdots O11	157(3)	
	O13 \cdots O12	2.975(4)	O13-H13A \cdots O12	129(3)	
	O14 \cdots O1	3.024(4)	O14-H14A \cdots O1	140(3)	
	O14 \cdots O2	2.762(4)	O14-H14A \cdots O2	148(3)	
	O14 \cdots O3	2.809(3)	O14-H14B \cdots O3	153(3)	
	O14 \cdots O4	3.059(4)	O14-H14B \cdots O4	132(3)	
Complex 4	O9 \cdots O5	2.963(3)	O9-H9B \cdots O5	138(2)	
	O9 \cdots O6	2.820(2)	O9-H9B \cdots O6	150(2)	
	O9 \cdots O7	2.872(3)	O9-H9A \cdots O7	135(3)	
	O9 \cdots O8	2.971(3)	O9-H9A \cdots O8	154(3)	

3-Magnetic data.

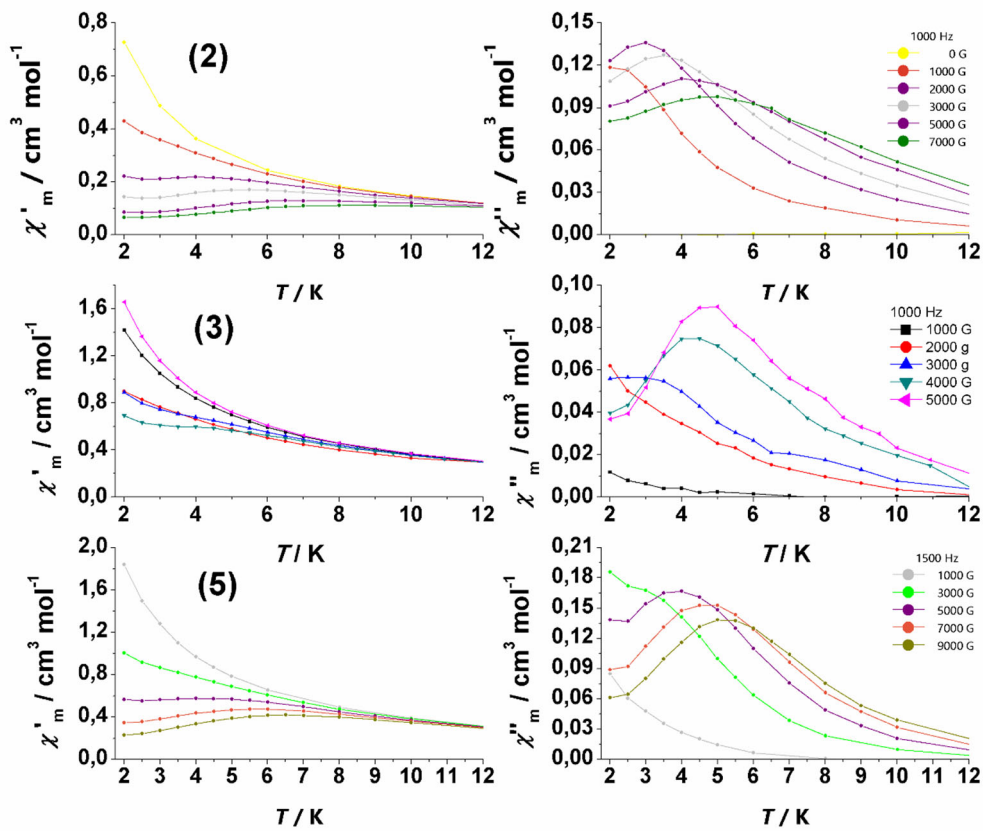


Fig. S3. χ_M'' dependence of the transverse field for complexes **2** (top), **3** (middle) and **5** (bottom).

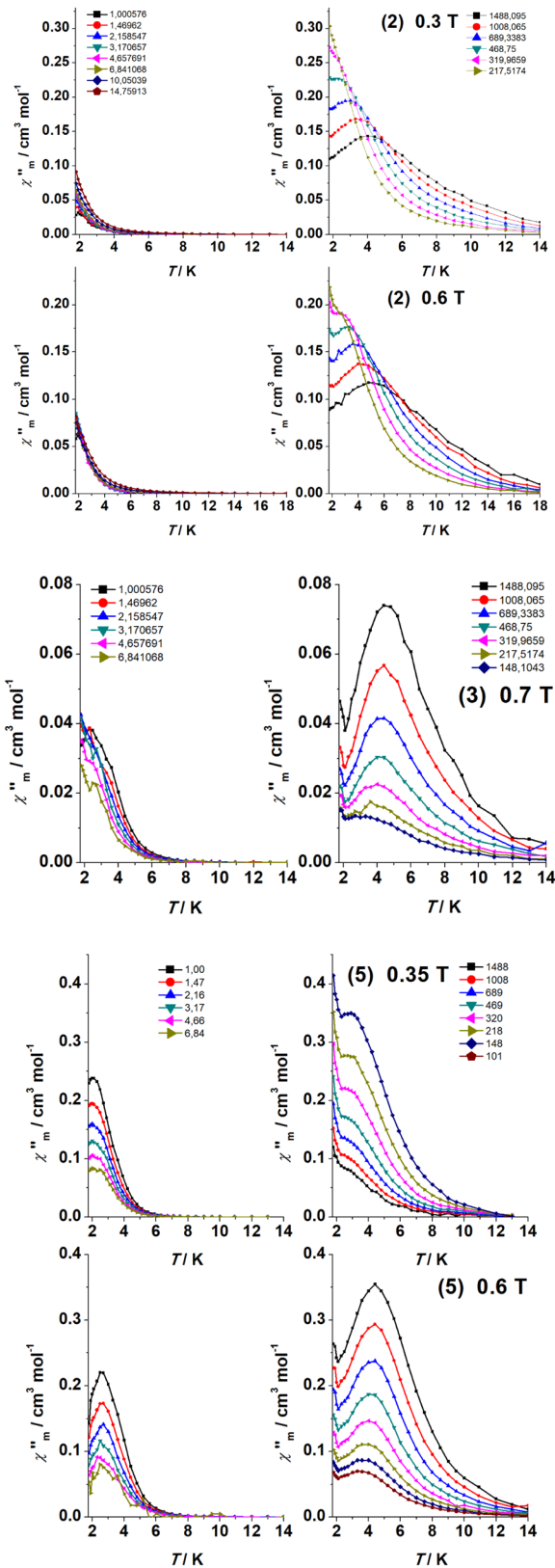


Fig. S4. $\chi''_m(T)$ for complexes **2**, **3** and **5** showing the lower frequencies (left) and temperature dependent high frequencies (right) out-of-phase response. For the intermediate range of frequencies maxima are not defined.

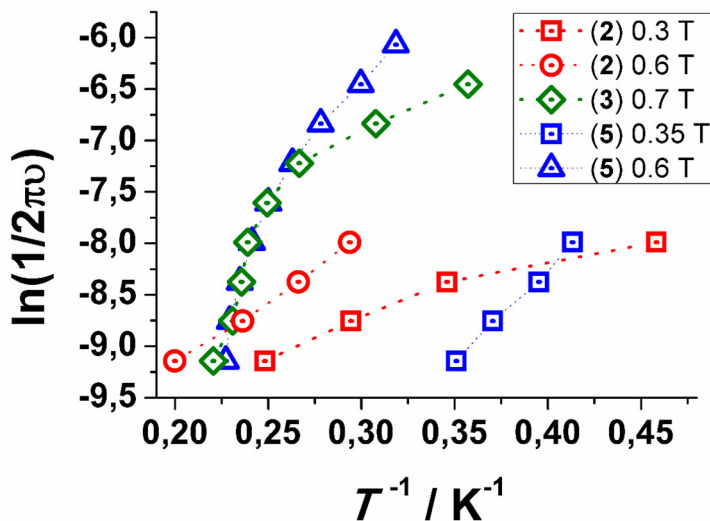


Fig. S5. Plot of $\ln(1/2\pi\nu)$ vs. T^{-1} from the $\chi''_m(T)$ data for complexes **2** (red), **3** (green) and **5** (blue). The data is limited to the HF region for which the maxima of χ''_m can be observed.

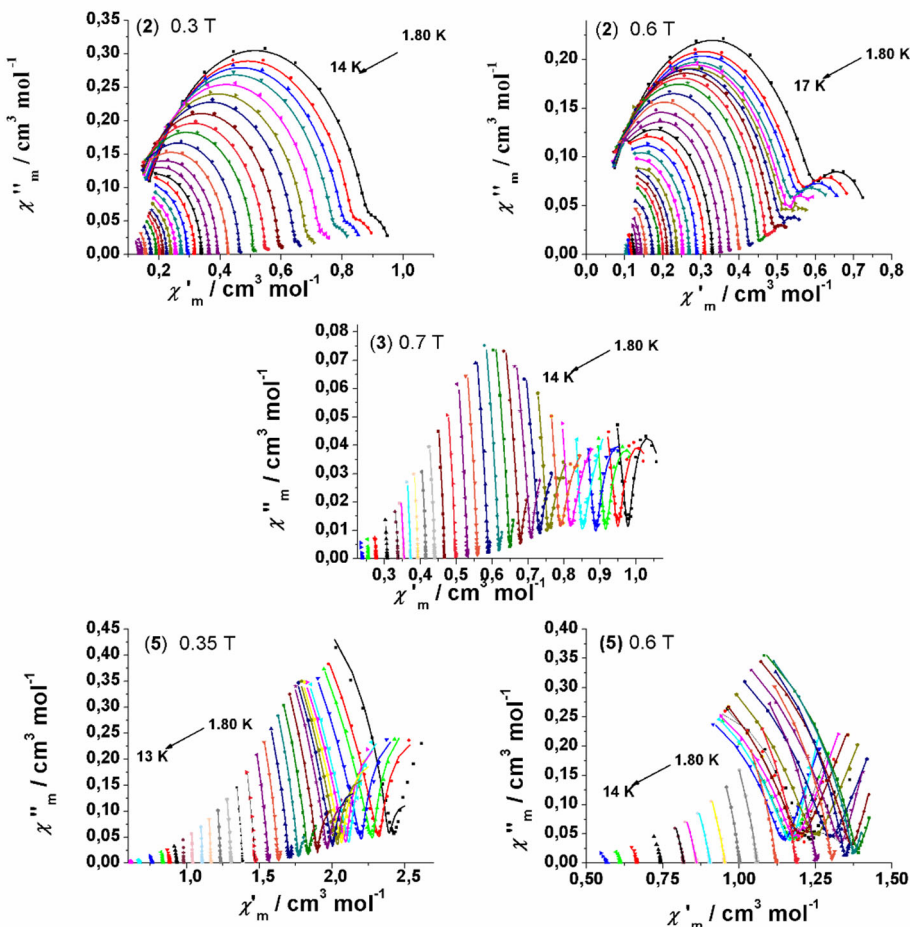


Fig. S6. Cole-Cole plots for complexes **2**, **3** and **5**. Solid lines show the best fit of the experimental data.